A NOVEL LABORATORY METHOD FOR DETERMINING CAPILLARY PRESSURE AND WETTABILITY WHILE MEASURING STEADY-STATE RELATIVE PERMEABILITY

Robin Gupta, Daniel Maloney, David Laverick, Robert Longoria, Larry Poore and Jeff Spitzenberger, ExxonMobil Upstream Research Company

This paper was prepared for presentation at the International Symposium of the Society of Core Analysts held in Snowmass, Colorado, USA, 21-26 August 2016

ABSTRACT

A novel laboratory method was developed that obtains relative permeability (k_r), capillary pressure (P_c), and wettability characteristics from a single reservoir-condition steady-state coreflood test. The method uses a modified inlet end-piece that isolates injection phases so that the difference between injection phase entry pressures is measured. Several inlet end-piece designs and related instrumentation are developed that can isolate and precisely capture the pressure difference of injection phases at the inlet. A method is developed to extract the capillary pressure from the difference in flowing injection phase pressures, which has both capillary and viscous pressure contributions. For this method, injected phase pressures are measured for several total flow rates for each steady-state fractional flow. This process enables quantification of P_c and k_r at each steady-state fractional flow condition. Rock wettability can be estimated from such measurements using either USBM or Amott-Harvey methods when the steady-state test includes both primary imbibition and secondary drainage cycles. Measured steady-state live-fluid coreflood data is used to illustrate this method of gaining both P_c and k_r functions from a single test. An excellent match was obtained between P_c quantified by the centrifuge method and the new method.

INTRODUCTION

Capillary pressure (Pc), relative permeability (kr) and wettability are key special core analysis (SCAL) characteristics used for reservoir performance predictions. Common practice is to measure these characteristics independently via several tests. Ideally, one would like to obtain all of these characteristics for a rock and fluid system from one test, saving time and cost. By doing so, a number of technical issues are avoided, such as mismatched data sets, anomalies from using different samples, test conditions, and fluids in the various tests, and propagation of errors from combining results from different tests.

When a sample (core plug or composite of core plugs) is mounted for a steady-state coreflood test, it is placed between inlet and outlet flow distribution end-pieces. The end-pieces serve as interfaces between the sample and upstream and downstream flow lines. During a two-phase steady-state flow measurement, two fluids are injected into and produced from the sample until steady-state is attained, that is, until saturation and

pressure drop across the length of the sample stabilize. The difference in phase pressures is close to zero at the outlet of the sample because of the capillary end-effect phenomenon (CEE). The difference between phase pressures is non-zero at the core inlet. From independent measures of injected phase pressures, one could conceptually determine capillary pressure as the difference between the non-wetting and wetting phase pressures. This is typically not practical because of phase mixing. This work addresses the mixing issue, enabling measures of phase pressures at the sample inlet face.

In a steady-state test, ability to measure differences in injection phase pressures at the sample inlet and to correct such measurements for viscous effects enables interpretation of capillary pressure. Thus, this work is an effort towards measuring relative permeability and capillary pressure curves on the same core plug (or first of a series of stacked plugs) simultaneously. Wettability can be calculated using established methods such as the Amott and the USBM (US Bureau of Mines) wettability index methods if both imbibition and secondary drainage capillary pressure cycles are available. Combining relative permeability, capillary pressure and wettability measurements into one test can yield a significant reduction in experimental time compared to measuring each separately.

Much of the previous work (for example, Longeron *et al.*, 1995; Richardson et al. 1952; Jennings *et al.*, 1988, Virnovsky *et al.*, 1995a, Virnovsky *et al.*, 1995b) relates to independent phase pressure measurements at the sample inlet using hydrophobic (oil-wet) and hydrophilic (water-wet) porous disks or membranes. For such approaches, properties of the disk or membrane allow pressure communication with one phase while the other phase is excluded. Drawbacks include the difficulty of initiating a reservoir-condition live fluid test without exceeding excluded-phase entry pressures of the porous disks or membranes, and uncertainty about whether or not the disk or membrane will perform as desired throughout the test. This work seeks to isolate the injection phases physically for phase pressure measurement rather than isolation via disks and membranes.

Authors including Richardson *et al.* (1952) and Gupta and Maloney (2015) suggested that capillary pressure may be quantified as the difference between non-wetting and wetting fluid phase pressures at the inlet. However, they did not account for the need to correct the viscous flow contribution to the pressure difference, which this work addresses. They also did not describe a practical inlet end-piece design to accomplish phase pressure measurements. Richardson *et al.* (1952) stated that the difference between non-wetting and wetting phase pressures at any point within porous media equals the capillary pressure corresponding to the saturation at that point. They demonstrated the concept by cementing gas (non-wetting) pressure probes to the rubber sleeve and oil (wetting phase) pressure probes made of ceramic porous media to core walls. Their experiments showed that the pressure difference between the non-wetting and wetting fluid phases inside the core is constant away from the outlet end and equals capillary pressure. Cementing probes on a sample is not a preferred approach because the practice might damage the sample or alter its wettability. Further, cementing probes for each test could be time intensive and susceptible to leaks.

Kokkedee (1994) and Pini (2013) proposed that capillary pressure is equal to pressure drop across the core at low rates. No special end-piece is required in this technique. However, this technique assumes that viscous forces are small compared to capillary forces, which may not be true in many test conditions. In this work, a method to correct viscous forces from inlet phase pressure is used to estimate capillary pressure.

APPARATUS DESIGN

Design elements of the proof of concept apparatus are shown in Diagram 1. In this design, end screens at the upstream face of the sample ordinarily used to promote mixing of injection phases are omitted. The inlet face of the sample is directly in contact with the inlet end-piece. To accurately measure difference in phase pressures at the inlet, two differential pressure transducers (high and low pressure ranges) are used in parallel, which can be engaged or disengaged depending upon the magnitude of the pressure difference. Pressures are also measured with Quartz absolute pressure transducers to provide redundancy. Pressure taps are placed as close as possible to the core holder inlet to minimize pressure drops from flow in the tubing and are placed at the same height to avoid gravity head differences. It is preferred to have check valves upstream of the inlet side pressure transducers to prevent back flow, which could result in phase mixing. As in a conventional flow system design, a differential pressure transducer or pair of Quartz absolute pressure transducers is used to measure pressure drop across the length of the sample. Pore pressure is maintained via closed-loop flow or by using a back pressure regulator (BPR). Overburden pressure is supplied by a pump.

INLET END-PIECE DESIGNS

Designing an inlet end-piece that is robust and prevents injection phase mixing at rock and end-piece junction is a challenging problem. Conventional inlet end-pieces have patterns that promote distribution of fluid phases. Examples of several conventional end-pieces are shown in Figure 1. Because test samples are porous, it is challenging to obtain a good seal between a metallic end-piece and a rock sample. Small scale irregularities on the rock surface and the smooth metal pattern on inlet end-pieces seal imperfectly, resulting in mixing of injected fluids and equilibration of their pressures. The challenge of obtaining a good seal and phase isolation exists even for a metal-based inlet end-piece with flow distribution patterns that do not intersect (Figure 1b and Figure 1c). To demonstrate this challenge, steady-state coreflood tests were performed on Cordova Cream limestone (7-9 mD) using helium gas and brine (20000 ppm) at room temperature, 1500 psi pore pressure, and 2400 psi net confining stress. Metal inlet end-pieces like those of Figure 1 were used. Capillary pressure was measured on a companion plug using the centrifuge method with the same net confining stress and temperature conditions. The modified flow apparatus, as discussed above, was used to perform this experiment. The steady-state coreflood was performed with multiple gas-water fractional flows. Pressure and saturation values were recorded at steady-state for each fractional flow. Figure 2 compares difference of inlet phase pressures for each fractional flow with centrifuge capillary pressure data. Clearly, no inlet phase pressure difference (ΔP) at steady-state conditions was measured when using a metal-based inlet end-piece, indicating phase

mixing at the inlet face of the sample. Similar results were observed from a repeat test using a screen between the inlet end-piece and core.

New end-piece designs were tested with the aim of finding a configuration that prevents phase mixing at the core inlet. New designs used machined metal end-pieces and elastomer seals. The metal is used to provide: 1) a desired pattern for fluid distribution, and 2) a rigid base for an elastomer seal that maintains structural integrity at high pressures. The elastomer in the design is used to seal between the inlet end-piece and sample surface to prevent phase mixing. The elastomer and metal/alloy needs to withstand test conditions. Examples of a few end-piece designs are shown in Figure 3.

Although the combination of metal and elastomer can prevent phase mixing, some designs perform better than others. For example, designs with small flow apertures like the O-ring design (Figure 3a) provide excellent sealing between the inlet end-piece and core face, but at the cost of significant additional viscous pressure contribution to the inlet phase pressure. This additional viscous pressure contribution can exceed capillary pressures. It comes from an enlarged region of high injection fluid saturation inside the core near the inlet. Figure 4 shows Cordova Cream limestone results of pressure difference of inlet phases from tests with the O-ring design and metal-based designs. In this test, steady-state was attained with multiple total flow rates for two helium fraction flows (0.5 and 0.8). The pressure difference of helium and brine were non-zero, clearly indicating that the O-ring end-piece provided a good seal. However, helium-brine pressure differences at the inlet were of large negative magnitude compared to centrifuge capillary pressures. This resulted from the additional viscous pressure contribution due to the O-ring design's small inlet aperture. With the O-ring design, phase saturations expanded in a hemispherical pattern inside the core at phase inlet ports. Since brine viscosity is almost two orders of magnitude higher than helium viscosity, the viscous pressure drop near the brine end-piece port is significant compared to that of the helium port. For this reason, the difference in helium-brine inlet pressures makes it seem that capillary pressure is negative in Figure 4. Typical measurement techniques for capillary pressure are performed with no flow and negligible viscous pressure gradients. In this test, the range of measured phase pressure differences match closely with Darcy equation calculations for hemispherical flow in porous media. To remedy this problem, it appeared desirable to have an elastomer-based inlet end-piece with wider flow aperture to reduce the viscous pressure contribution in measured inlet phase pressures.

The use of an elastomer seal that withstands test fluids and conditions is important. Some elastomers may perform well at room conditions, but may lose structural integrity in the presence of hydrocarbons at high pressure and temperature. An example is shown in Figure 5 in which a spiral elastomer pattern made using an incompatible material was destroyed when exposed to live crude oil and brine at high temperature and pressure.

Inlet end-piece patterns with metal and elastomer (e.g., Half-moons and Spiral with gasket in Figure 3) tend to perform better than those with only elastomer between the end-piece and sample (e.g., Elastomer spiral). Elastomers are more compressible

compared to metal. In a 100% elastomer based design, if grooves are not sufficiently deep or wide, there is a risk of pattern distortion under high pressure. During another test with Cordova Cream limestone outcrop at 1500 psi pore pressure and 2400 psi net confining stress, an Elastomer spiral pattern was able to isolate phases at the inlet for the first 4000 minutes (Figure 6), but later failed as evidenced by the reduction in inlet phase pressures to zero as a result of phase mixing. Figure 7 shows post-test pictures of the core and end-piece. The salt residue from brine spreading over most of the inlet end-piece face (Figure 7a) and the brine streak connecting positions of injection ports for both phases on the rock face (Figure 7b) provide clear evidence that fluids mixed at the core face and did not remain isolated. The risk of having the elastomer lose structural integrity under high pressure can be reduced if the end-piece is made of both elastomer and metal.

Based on the above discussion, a good inlet end-piece design contains: 1) a wider aperture or surface area for injection phases to minimize the viscous pressure contribution in measured inlet phase pressures, 2) compatible elastomer material, and 3) face design consisting of both metal and elastomer, or 100% elastomer with sufficient groove width and depth. Examples of such end-pieces are the Spiral with gasket (Figure 3c) and Half-moons (Figure 3d).

From a similar experiment on Cordova Cream limestone outcrop, the Half-moon inlet end-piece successfully isolated both brine and helium phases. Figure 8 shows the difference of phase pressures at steady-state for multiple fractional flows and multiple rates at each fractional flow. Clearly, phase pressure differences at the inlet are non-zero, indicating successful isolation of injection phases at the face of the inlet end-piece. Further, the differences between phase pressures at the inlet are positive, indicating lower viscous contributions to the measurements because of better phase spreading at the core plug face (or wide injection cross section) compared to results from an end-piece with small injection aperture, such as the O-ring design. Though viscous contributions with the Half-Moon design are relatively low, they are not zero, which reflects flow rate dependence in the difference between inlet phase pressures. Because of viscous gradient effects, the difference in inlet phase pressures is lower than the static capillary pressure measured by the centrifuge method in Figure 8. Thus, the viscous contribution must be subtracted from the difference in inlet phase pressures to achieve a measure of capillary pressure from a steady-state coreflood test.

VISCOUS PRESSURE CORRECTION

The difference between non-wetting and wetting phase pressures at the inlet equals P_c only at a static condition (zero flow rate). However, in a coreflood test (both steady-state and unsteady-state), one or both phases are continuously injected, and the phase pressures at the inlet result from both capillary and viscous forces. Hence, a method is required to estimate and correct the viscous pressure contribution from the difference of phase pressures at the inlet.

In a steady-state coreflood test, corrections for viscous pressure contributions can be determined by performing tests at multiple flow rates for each fractional flow. Steady-

state is achieved at each flow rate. For a given fractional flow, capillary pressure is equal to the intercept of the trend line from a plot of steady-state phase pressure difference at the inlet versus total flow rate (Figure 9). Close to the inlet, fluid saturation does not change significantly with flow rates. Hence, phase pressure difference at the inlet changes linearly with total flow rate for a typical steady-state fractional flow condition, and the intercept of the linear trend equals capillary pressure. The capillary pressure measured using the above method corresponds to the capillary end-effect corrected fluid saturation, which can be estimated using the Intercept Method (Gupta and Maloney, 2015) or through in-situ saturation monitoring. In tests with sufficiently high pressure drop across the core, the correction might be small and within experimental accuracy, and the average saturation across the core can be used.

APPLICATION EXAMPLE AT RESERVOIR CONDITIONS

A water-oil steady-state coreflood test was performed using one of the new inlet end-pieces to demonstrate the concept of obtaining capillary pressure from the difference of phase pressures (after viscous pressure correction) at the inlet. This test was performed on native state core plugs stacked in series to make a composite of 25 cm length. The test was performed at reservoir temperature and reservoir pore and overburden pressures using live fluids. Viscosities of oil and brine were similar. Pressure measurement devices were configured as in Diagram 1. The "Half-Moons" inlet end-piece was used (Figure 3d). The test was an imbibition steady-state test, beginning with a measurement of oil permeability at irreducible water saturation and continuing with oil and water co-injection in steps of decreasing oil fractional flow (F_o). For each F_o, after achieving steady-state conditions, total flow rate was increased several times. With the direction of total flow rate increasing, unwanted hysteresis is avoided. When F_o is decreased for the next set of steady-state measurements, flow rate can be reduced concurrently with the fractional flow change. Because the change in oil fractional flow coincides with an increase in brine saturation, the reduction of total flow rate between consecutive fractional flows avoids or reduces potential for inadvertently introducing hysteresis because of saturation reversals.

Figure 10 shows phase pressure difference (oil minus brine phase pressure) at the inlet and total flow rate versus time. As discussed above, reductions in total flow rate on Figure 10 coincide with changes in fraction flow. In Figure 10, the difference in phase pressures at the inlet is non-zero and ranges from -10 to +10 psi. The "Half-Moons" end-piece was able to clearly prevent phase mixing at the inlet face during this test.

In theory, the capillary pressure contribution to the difference between measured phase pressures is insensitive to total flow rate. In Figure 10, the phase pressure difference at the inlet changes with flow rate at each fraction flow. This flow rate dependence is the result of viscous rather than capillary phenomena. Figure 11 plots oil phase pressure minus brine phase pressure at the inlet versus total flow rate from steady-state measurements with oil fractional flows of 0.985, 0.9 and 0.3. All three plots show linear trends, as do plots for the other fractional flows that are not shown. Intercepts equal capillary pressure, while slopes are influenced by viscous effects. Slopes are positive for

oil fractional flows above 0.5 (because oil rates are greater than brine rates) and negative for fractional flows below 0.5 (because brine rates are greater than oil rates).

Constructing the capillary pressure curve for the rock at the inlet consists of plotting the intercepts (from the phase pressure difference versus rate plots) versus the corresponding brine saturations. Brine saturation was calculated by applying the Intercept method (Gupta and Maloney, 2015), which corrects the steady-state data for capillary end-effects. Since pressure drops in this test were high, capillary end-effect corrections to brine saturations were small. Figure 12 shows the resulting capillary pressure plot for this test. Saturations at the first and last points represent residual brine and residual oil saturations for this test. In theory, capillary pressure curves asymptote at residual saturations at both ends, but values of 11 psi and -15 psi were used to denote the capillary pressures at these residual saturations. This plot closely matches the centrifuge capillary pressure curves measured on preserved companion plugs of the same rock type (Figure 12), particularly with core sample C1. Figure 13 shows pore throat size distributions for the centrifuge core plugs (C1 to C4) and inlet-plug (S1) of the steady-state test. Clearly, plug C1 pore throat size and imbibition centrifuge capillary pressure data is closest to core plug S1 used in the steady-state test. The k_r curve obtained in this test closely matched with the curve obtained on samples with similar geology.

Overall, the new method is easy to implement and only requires minor modifications to a steady-state apparatus along with using a modified inlet end-piece. Even if an end-piece fails to prevent phase mixing during a test, quality steady-state relative permeability data is still obtained. However, this method has certain challenges. For example, the inlet end-piece design should be robust and needs to prevent phase mixing throughout the test, the test duration is slightly increased due to multiple flow rates performed for each fractional flow, and viscous pressure correction needs to be added to the test workflow. The application for a gas-liquid system is relatively more challenging compared to a liquid-liquid system because of low gas viscosity. A gas is more susceptible to leaks and phase mixing and generates relatively high viscosity pressure correction compared to a liquid.

CONCLUSION

Modified inlet end-pieces described in this work successfully isolated injected phases in a coreflood test, allowing measurement of inlet phase pressures. The inlet phase pressures at steady-state conditions were used to estimate capillary pressure of the core after applying viscous pressure corrections. If both imbibition and secondary drainage cycles are performed during a steady-state test, then capillary pressures as well as relative permeabilities can also be measured. Wettability of the core can be inferred from imbibition and secondary drainage capillary pressure curves using either Amott or USBM wettability index methods. Thus, using the described inlet end-piece designs and test methodology, relative permeability, capillary pressure and wettability of a core can be measured simultaneously in a single steady-state test, which may result in significant time and cost savings.

REFERENCES

1. Richardson, J. G., Kerver, J. K., Hafford, J. A. and Osoba, J. S. (1952, August 1). Laboratory Determination of Relative Permeability. Society of Petroleum Engineers. doi:10.2118/952187-G
2. Longeron, D., Hammervold, W. L. and Skjaeveland, S. M. (1995, January 1). Water-Oil Capillary Pressure and Wettability Measurements Using Micropore Membrane Technique. Society of Petroleum Engineers. doi:10.2118/30006-MS
3. Virnovsky, G.A., Guo, Y. and Skjaeveland, S.M. (1995a, May 15). Relative Permeability and Capillary Pressure Concurrently Determined from Steady - State Flow Experiments. 8th. European IOR - Symposium in Vienna, Austria
4. Virnovsky, G.A., Guo, Y., Skjaeveland, S.M. and Ingsoy, P (1995b, October). Steady-State Relative Permeability Measurements and Interpretation with Account for Capillary Effects. Society of Core Analysts Conference in San Francisco, USA
5. Gupta, R., and Maloney, D. R. (2015, December 1). Intercept Method--A Novel Technique To Correct Steady-State Relative Permeability Data for Capillary End Effects. Society of Petroleum Engineers. doi:10.2118/171797-PA
6. Kokkedee, J. A. (1994, January 1). Simultaneous Determination of Capillary Pressure and Relative Permeability of a Displaced Phase. Society of Petroleum Engineers. doi:10.2118/28827-MS
7. Pini, R., and Benson, S.M.. 2013. "Simultaneous Determination of Capillary Pressure and Relative Permeability Curves from Core-Flooding Experiments with Various Fluid Pairs." Water Resources Research 49 (6): 3516–30. doi: 10.1002/wrcr.20274

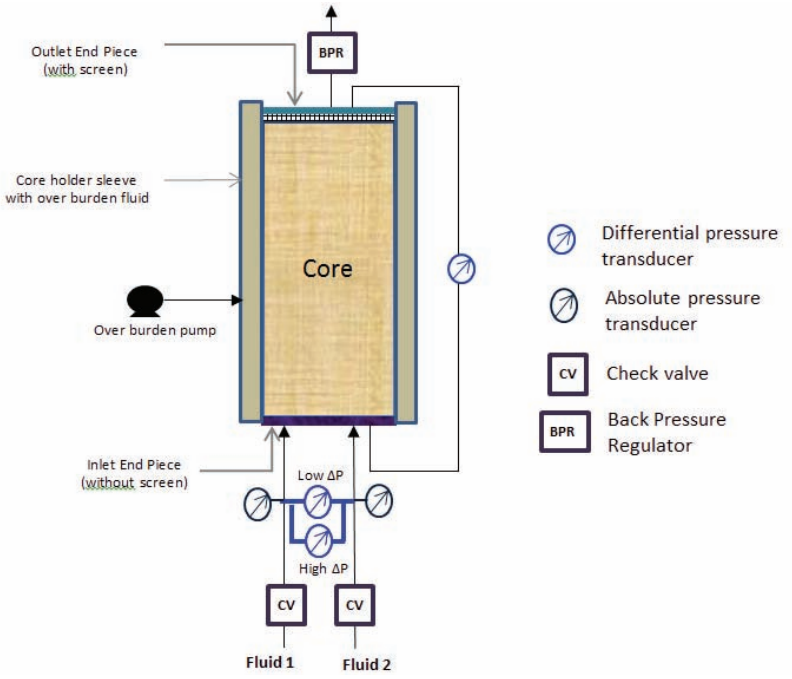

Diagram 1: Schematic of modified core holder assembly

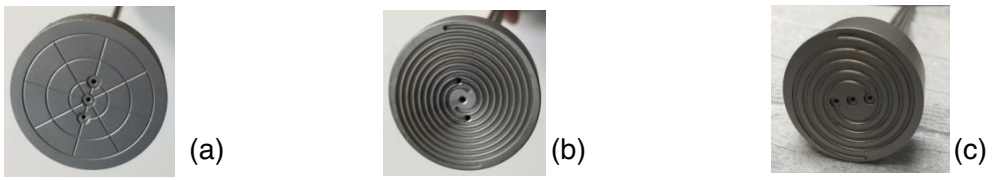

Figure 1: Examples of conventional inlet end-piece designs: (a) Cross, (b) Spiral, and (c) Modified spiral

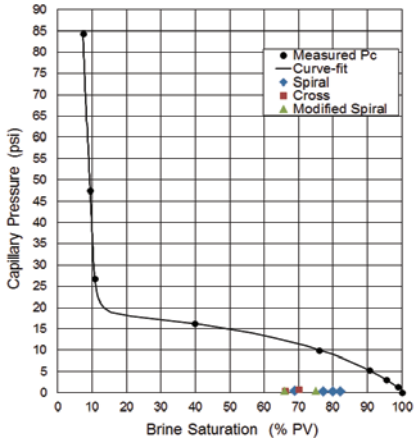

Figure 2: Difference of inlet phase pressure compared to measured capillary pressure for Cross, Spiral and Modified spiral inlet end-pieces

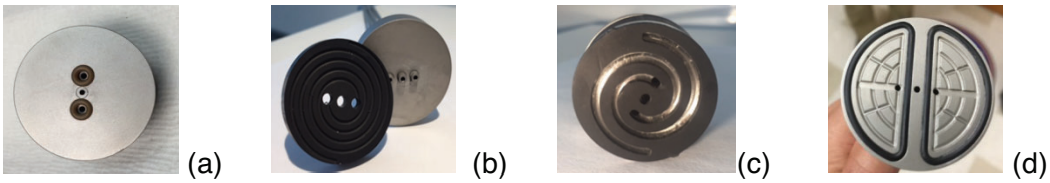

Figure 3: Examples of new elastomer based inlet end-piece designs, (a) O-ring, (b) Elastomer spiral, (c), Spiral with gasket, and (d) Half-moons

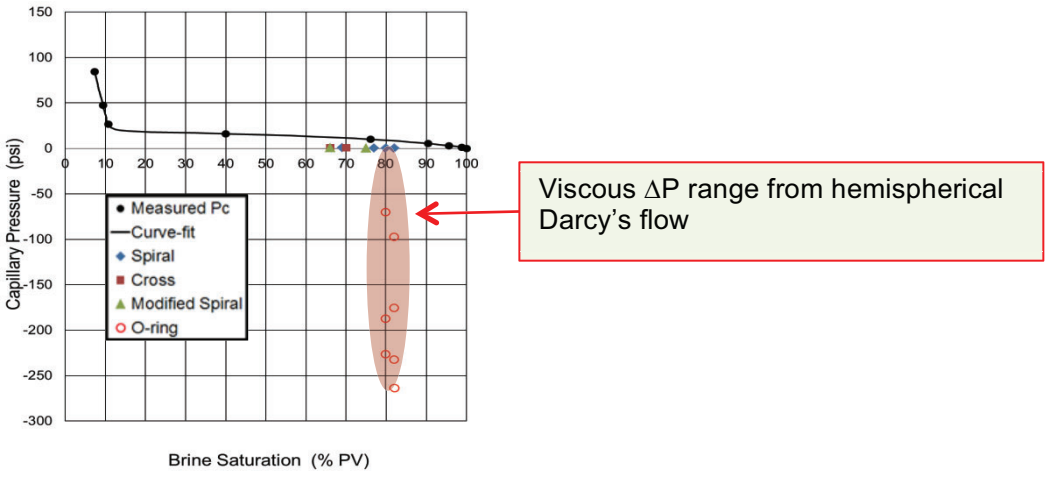

Figure 4: Difference of inlet phase pressure compared to measured capillary pressure for Cross, Spiral, Modified spiral and O-ring inlet end-pieces

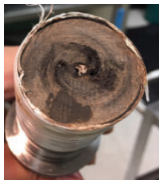

Figure 5: Spiral with gasket end-piece after exposure to live crude oil at high pressure and temperature. Incompatible material was used in this test.

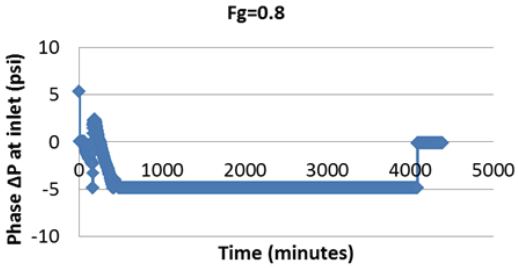

Figure 6: Plot of difference in inlet phase pressures with time for helium-brine steady-state test with Elastomer spiral inlet end-piece

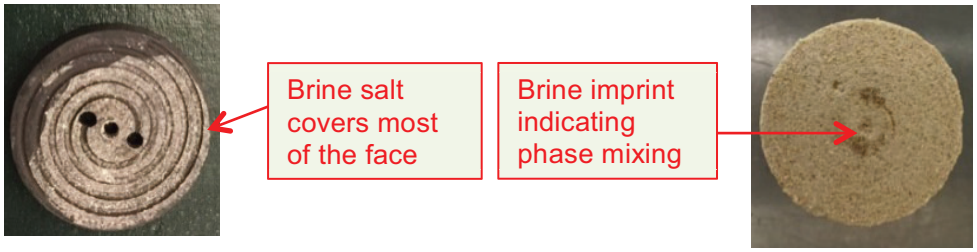

Figure 7: Pictures taken after the test for, (a) face of Elastomer spiral inlet end-piece, and (b) face of the core at the inlet side

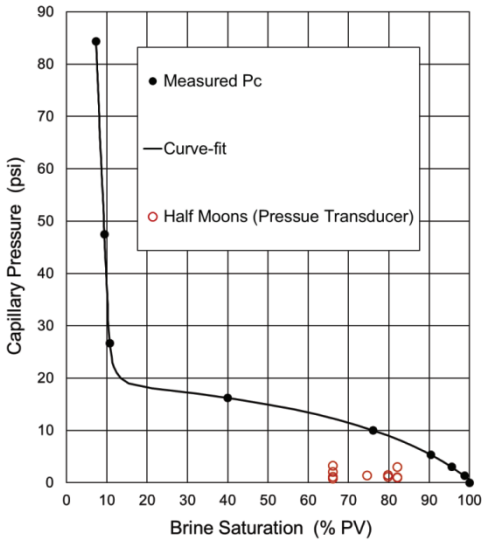

Figure 8: Difference of inlet phase pressures from Half-Moons end-piece compared to measured capillary pressure

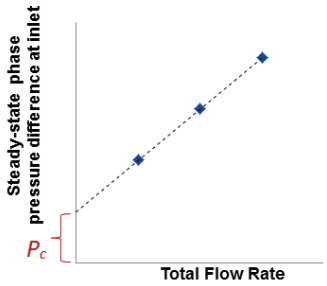

Figure 9: Plot of steady-state phase pressure difference at inlet with total flow rate for a given fractional flow. The intercept of the trend line of this plot equals static capillary pressure.

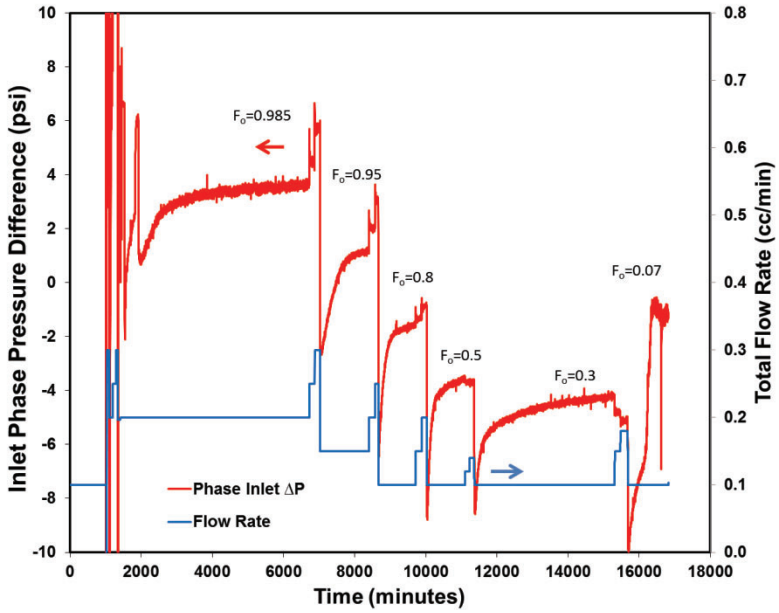

Figure 10: Difference in phase pressure at inlet and total flow rate with time at different oil fractional flow (Fo)

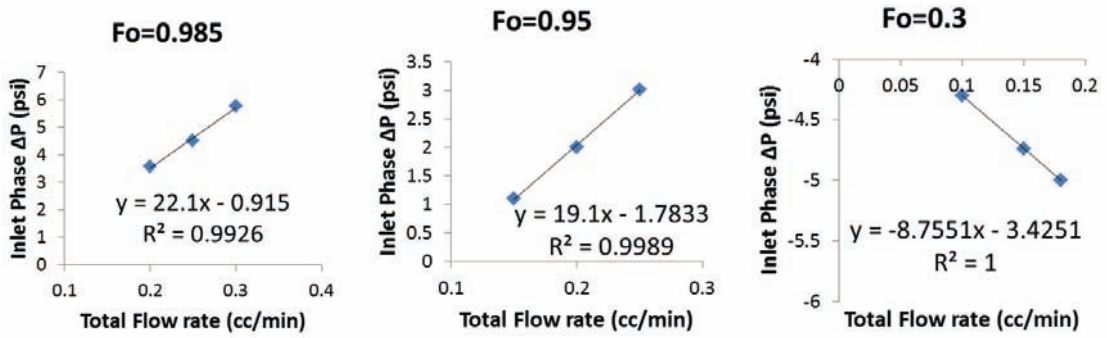

Figure 11: Plot of inlet phase pressure difference at steady-state condition with total flow rate for oil fractional flows of 0.985, 0.95 and 0.3. All three plots have linear trends. Intercepts equal capillary pressures.

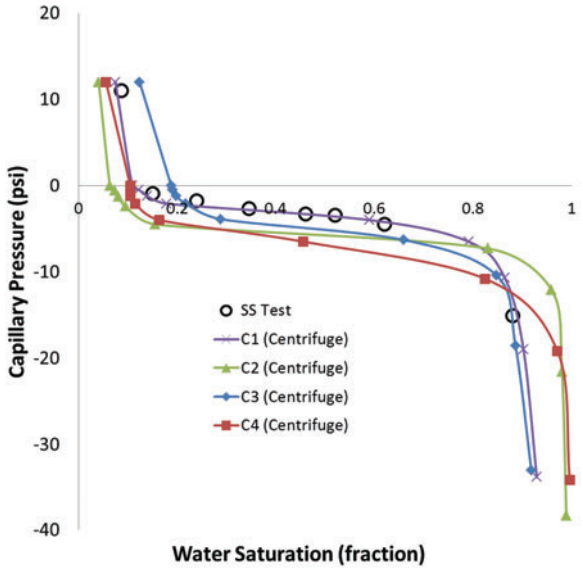

Figure 12: Capillary pressure curve obtained using the new method and compared with centrifuge capillary pressure measured on preserved plugs (C1 -C4) of the same rock type

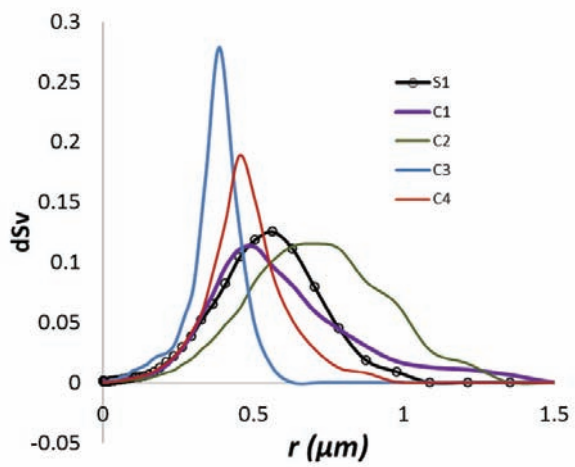

Figure 13: Pore throat size distribution for the inlet core plug used in the steady-state test and the four core plugs for same rock type used in the centrifuge capillary pressure test